

Published in final edited form as:

Biochem Pharmacol. 2013 March 15; 85(6): 839–848. doi:10.1016/j.bcp.2012.11.018.

Cloning, expression and analysis of the olfactory glutathione S-transferases in coho salmon

Herbert M. Espinoza¹, Laura M. Shireman², Valerie McClain¹, William Atkins², and Evan P. Gallagher^{1,*}

¹Department of Environmental and Occupational Health Sciences, University of Washington, Seattle, WA

²Department of Medicinal Chemistry, University of Washington, Seattle, WA

Abstract

The glutathione S-transferases (GSTs) provide cellular protection by detoxifying xenobiotics, maintaining redox status, and modulating secondary messengers, all of which are critical to maintaining olfaction in salmonids. Here, we characterized the major coho salmon olfactory GSTs (OlfGSTs), namely omega, pi, and rho subclasses. *OlfGST omega* contained an open reading frame of 720 bp and encoded a protein of 239 amino acids. *OlfGST pi* and *OlfGST rho* contained open reading frames of 727 and 681 bp, respectively, and encoded proteins of 208 and 226 amino acids. Whole-protein mass spectrometry yielded molecular weights of 29,950, 23,354, and 26,655 Da, respectively, for the GST omega, pi, and rho subunits. Homology modeling using four protein-structure prediction algorithms suggest that the active sites in all three OlfGST isoforms resembled counterparts in other species. The olfactory GSTs conjugated prototypical GST substrates, but only OlfGST rho catalyzed the demethylation of the pesticide methyl parathion. OlfGST pi and rho exhibited thiol oxidoreductase activity towards 2-hydroxyethyl disulfide (2-HEDS) and conjugated 4-hydroxynonenal (HNE), a toxic aldehyde with neurodegenerative properties. The kinetic parameters for OlfGST pi conjugation of HNE were $K_M = 0.16 \pm 0.06$ mM and $V_{max} = 0.5 \pm 0.1 \mu\text{mol min}^{-1} \text{mg}^{-1}$ for OlfGST pi, whereas OlfGST rho was more efficient at catalyzing HNE conjugation ($K_M = 0.022 \pm 0.008$ mM and $V_{max} = 0.47 \pm 0.05 \mu\text{mol min}^{-1} \text{mg}^{-1}$). Our findings indicate that the peripheral olfactory system of coho expresses GST isoforms that detoxify certain electrophiles and pesticides and that help maintain redox status and signal transduction.

Keywords

glutathione S-transferases; coho salmon; olfaction; 4-hydroxynonenal; oxidative stress; methyl parathion

© 2012 Elsevier Inc. All rights reserved.

*Corresponding author: Department of Environmental and Occupational Health Sciences, School of Public Health, 4225 Roosevelt Way NE, Suite 100, Seattle, WA 98105 – 6099, United States, Telephone: 1-206-616-4739, Fax: 1-206-685-4696, evang3@uw.edu.

Publisher's Disclaimer: This is a PDF file of an unedited manuscript that has been accepted for publication. As a service to our customers we are providing this early version of the manuscript. The manuscript will undergo copyediting, typesetting, and review of the resulting proof before it is published in its final citable form. Please note that during the production process errors may be discovered which could affect the content, and all legal disclaimers that apply to the journal pertain.

1. Introduction

The glutathione *S*-transferases (GSTs) are a multifunctional family of phase II detoxification enzymes that protect cells against harmful endogenous toxic metabolites, superoxide radicals, and exogenous toxic chemicals [1–3]. To date, at least 14 classes of mammalian GSTs have been identified based on primary amino acid sequences with GSTs sharing more than 40% identity being assigned to the same class, and those sharing less than 30% being assigned to different classes [4]. Additionally, the structurally distinct membrane-bound microsomal GSTs are a separate GST subfamily belonging to the Membrane Associated Proteins in Eicosanoid and Glutathione (MAPEG) metabolism pathway [5]. Although the predominant catalytic activity of GSTs involves the conjugation of exogenous and endogenous compounds by facilitating nucleophilic attack by reduced glutathione (GSH), several GSTs combat oxidative stress by GSH-dependent peroxidase activity or via conjugation of reactive α - β -unsaturated aldehydes produced during lipid peroxidation. In addition, certain environmental chemicals or their metabolites are also GST substrates, and species' differences in GST expression have been linked to susceptibility to chemical injury [6].

Although fish GSTs have not been well characterized relative to mammals, all fish have GST activity and express multiple GST isoforms. The predominant GST in carp (cyprinids), salmon (salmonids) and cod (gadoids) is a pi class GST (GST pi), whereas the major isoform in flatfish (pleuronectids), mullet (mugilids), sea bream (sparids) and bass (centrarchids) is a rho class GST [7]. Coho salmon exhibit a complex GST tissue profile encompassing 9 subfamilies, including alpha, mu, pi, theta, omega, kappa, rho, zeta and microsomal GSTs [8, 9] and have notable tissue differences in constitutive expression patterns [8]. For example, omega-, pi-, and rho-class GST mRNA transcripts predominate in the olfactory system of coho salmon, and of the three forms, rho GSTs are an evolutionarily distinct subclass of GSTs restricted to aquatic organisms. Rho GSTs were initially characterized in pleuronectid flatfish and largemouth bass [10] and originally misidentified as theta-class-like GSTs [11]. As a group, rho GSTs share >80% homology among aquatic animals [12], and can dominate total tissue GST composition [13]. Although the endogenous function of rho GSTs has not been determined, rho GSTs from several aquatic species conjugate 4-hydroxynonenal (HNE) [7], a reactive aldehyde produced during lipid peroxidation. Fish can be particularly vulnerable to membrane damage due to high levels of polyunsaturated fatty acids that are susceptible to peroxidation. Accordingly, GST rho may have functionality in protecting fish tissues against oxidative damage associated with changes in membrane fluidity. Furthermore, the fact that HNE also exhibits neurodegenerative properties suggests that the expression of HNE-conjugating GSTs, such as GST rho, in the peripheral or central nervous system tissues of fish is also of physiological importance. However, not all rho GSTs exhibit HNE conjugating activity, suggesting that minor differences in protein structure can markedly affect HNE catalytic specificity. Notwithstanding, the fact that HNE plays a major role in oxidative stress-induced signaling indicates that certain GST isoforms that are active in HNE metabolism may also regulate cellular signal transduction.

Although fish GSTs have been studied most in liver tissues, the peripheral olfactory system is in direct contact with the environment and is vulnerable to waterborne chemical exposures. For this reason, maintenance of intact olfaction in the presence of chemical exposures is critical for uninterrupted olfactory signaling, which in turn triggers sensory motor-dependent functions (i.e. predator avoidance, prey selection, and homing) critical to survival [14–17]. The present study describes the identification, expression and catalytic function of the three major olfactory GST isoforms in coho salmon. We were particularly interested in understanding the role of GSTs in mediating the effects of oxidative stress and

the metabolism of HNE due to its critical role in cellular oxidative damage as well as mediating signal transduction processes that may be important in salmon olfaction.

2. Materials and Methods

2.1 Chemicals

MS-222 (Tricaine methanesulfonate) was obtained from Argent Chemical Laboratories (Redmond, WA). TRIzol® reagent, the SuperScript® First-Strand Synthesis System, and the Zero Blunt® TOPO® PCR Cloning Kit for Sequencing were purchased from Invitrogen (Carlsbad, CA). Finnzymes Phusion® Hot Start was purchased from Thermo Fisher Scientific, (Waltham, MA). T4 DNA Ligase and all cloning restriction endonucleases were purchased from New England Biolabs, Inc. (Ipswich, MA). The SMART™ RACE cDNA Amplification Kit was obtained from Clontech (Mountain View, CA). Primers were obtained from Eurofins MWG Operon (Huntsville, AL). The pET-28a (+) vector, the E. coli bacterial strain BL21 DE3, and restriction grade Thrombin Protease were obtained from Novagen (Madison, WI). Ni Sepharose™ High Performance Beads were purchased from GE Healthcare (Pittsburg, PA). Ampicillin, kanamycin, isopropyl β-D-1-thiogalactopyranoside (IPTG), imidazole, 1-chloro-2,4-dinitrobenzene (CDNB), 2,4-dichloro-nitrobenzene (DCNB), ethacrynic acid (ECA), cumene hydroperoxide (CuOOH), 2-hydroxyethyl disulfide (2-HEDS), methyl parathion, and reduced GSH were purchased from Sigma (St. Louis, MO). HNE was purchased from Cayman Chemicals (Ann Arbor, MI). Glutathionyl 4-hydroxynonanal (GSHNE) was biosynthesized as described previously [18]. All other chemicals and solvents were of analytical grade and purchased from standard sources (Thermo Fisher Scientific, Waltham, MA; Sigma, St. Louis, MO).

2.2 Animals and tissue processing

Juvenile coho salmon (~1 year of age) were provided by the National Oceanic and Atmospheric Administration (NOAA), Seattle, WA. Fish were raised in cylindrical tanks with recirculated freshwater under natural photoperiod in dechlorinated municipal water and fed commercial dry food pellets (BioOregon, Warrenton, OR, USA) daily. Animal welfare and experimental procedures were carried out in strict accordance with the University of Washington Institutional Animal Care and Use Committee (IACUC) guidelines. For RNA preparations, olfactory rosettes were collected from individuals euthanized with MS-222 (Argent Chemical Laboratories, Redmond, WA), rinsed in 1× PBS (pH 7.0), placed in 1 mL Trizol, and snap-frozen in liquid nitrogen. For subcellular preparations, olfactory rosettes were pooled from 20 juvenile coho, rinsed in 1× PBS (pH 7.0), and snap-frozen in liquid nitrogen. For catalytic activity analysis, liver tissue was collected from juvenile coho salmon, snap-frozen in liquid nitrogen, and stored at -80 °C until processing.

2.3 Cloning of olfactory GST isoforms by RACE

An olfactory cDNA library was synthesized from 1 μg of total RNA (DNase treated) using oligo (dT) primers and Superscript II reverse transcriptase (Invitrogen, Carlsbad, CA). Rapid amplification of cDNA ends (RACE-PCR) using the SMART™ RACE cDNA Amplification Kit (Clontech, Mountain View, CA) together with MMLV Reverse Transcriptase (Clontech, Mountain View, CA) was used to amplify the *GST omega*, *pi*, and *rho* partial cDNAs according to the supplier's protocol. Gene-specific RACE primers for *GST pi* were designed against *Salmo salar GST pi* full-length sequence (Table 1). Primers for *GST rho* were designed against both *Oncorhynchus mykiss* and *Salmo salar GST A* full length sequences (Table 1). Similarly, gene-specific RACE primers for *GST omega* were designed against *Oncorhynchus mykiss* and *Salmo salar GST omega 1* full-length sequences (Table 1).

All amplified PCR products were cloned into the pCR4Blunt-TOPO cloning vector (Invitrogen, Carlsbad, CA) and sequenced at the University of Washington, Department of Biochemistry Sequencing Facility. Nucleotide and deduced amino acid sequences were compared to all databases available on the National Center for Biotechnology Information site (NCBI at www.ncbi.nlm.nih.gov) using Basic Local Alignment Search Tool (BLAST) programs, whereas sequence alignments and phylogenetic analyses were performed using ClustalW (San Diego Biology Workbench 3.2, <http://workbench.sdsc.edu/>) and Molecular Evolutionary Genetics Analysis (MEGA5; [19]) respectively. The final contiguous sequences were compiled using DNASTAR Lasergene8 sequence analysis software (DNASTAR, Madison, WI).

2.4 Heterologous expression and protein purification

OlfGST omega, *pi*, and *rho* cDNAs were constructed via PCR sewing using Phusion® Hot Start (Thermo Fisher Scientific, Waltham, MA). Briefly, unique *NheI* and *HindIII* restriction sites were engineered into the 5' and 3' ends (respectively) of validated pCR4Blunt-TOPO-GST RACE using the primers listed in Table 1. The touchdown PCR profile for the PCR amplification was 30 s at 98 °C (1 cycle); 98 °C for 10 s, 68-58°C 30 s, 72 °C for 30 s (35 cycles total); 5 min at 72 °C (1 cycle). Following restriction digest, inserts were ligated into the pET-28a (+) vector (Novagen, Madison, WI) in frame with, and immediately downstream of the thrombin cleavage site and a 6 histidine tag. Transformants were analyzed by a *NheI* and *HindIII* restriction digest and then subsequently sequenced.

pET-28a (+) His-GST plasmids were transformed into the BL21 DE3 cells and grown in Luria Broth (Thermo Fisher Scientific, Waltham, MA) supplemented with kanamycin (50 ug/ul). Cultures were induced with IPTG for 3–4 hs at 30 °C and the bacteria were lysed by sonication. After centrifugation, the supernatant was incubated for 1 h at 4 °C with 1 mL of Ni Sepharose™ beads equilibrated in buffer (20mM sodium phosphate buffer, 0.5 M NaCl, 40 mM imidazole, pH 7.4) to allow for efficient His-GST protein binding. The Ni bead column was sequentially washed in buffers with increasing concentrations of imidazole (20 mM sodium phosphate buffer, 0.5 M NaCl, 40–150 mM imidazole, pH 7.4) to remove nonspecific bacterial proteins. The His-GST/Ni bead slurry was resuspended in buffer (20 mM sodium phosphate buffer, 0.5 M NaCl, 40 mM imidazole, pH 7.4) and proteins were cleaved from the His moiety by incubating with thrombin protease (Novagen, Madison, WI). Supernatant was transferred to a Pierce Slide-A-Lyzer Dialysis Cassette 10K MWCO (ThermoScientific, Waltham, MA) and dialyzed at 4 °C in buffer (100 mM KPO₄, 1 mM EDTA, 2 mM DTT, 10% glycerol, pH 7.0). Samples were transferred from cassettes to chilled tubes and then incubated at 4 °C for 1 h with *p*-aminobenzamidine-agarose beads (Sigma, St. Louis, MO) equilibrated in dialysis buffer to remove histidine residues. In the case of GSTs omega and pi, the His moiety could not be cleaved by thrombin digest; therefore, the protein complex was eluded off with 200 mM imidazole and then dialyzed as described above. Recombinant proteins were aliquoted and stored at –80 °C until further use.

2.5 Whole-protein mass spectrometry analysis of OlfGST pi, omega, and rho subunits

To determine the whole-protein mass of OlfGSTs, purified protein was analyzed by liquid-chromatography/mass spectrometry (LC/MS) using the continuum format of data collection on a Waters Micromass Synapt ion-mobility time-of-flight mass spectrometer (Waters Corporation, Milford, MA). The instrument scanned from 500–2200 m/z with a scan time of 0.5 sec and a cone voltage of 20 V. A Waters Alliance 2690 high-pressure liquid-chromatography module (HPLC, Waters Corporation, Milford, MA) provided a flow rate of 0.3 mL/min using 70% A (water with 0.1% trifluoroacetic acid) and 30% B (acetonitrile with 0.1% trifluoroacetic acid) for the first 3 minutes of the run followed by a linear gradient

over 3.5 minutes to 65% B, a linear gradient over 0.5 min to 100% B, equilibration at 100% B for 2 min, and a linear gradient to 30% B over 0.1 min with the run ending at 10.5 min. Mass spectra were deconvoluted from 800–2000 m/z using the MaxEnt I algorithm within the Waters MassLynx v4.1 software package (Micromass Ltd., Milford, MA). The parameters for deconvolution were: 1 Da/channel resolution, uniform Gaussian damage model, 1 Da peak width at half height, iterated to convergence.

2.6 Protein structure prediction analysis

Secondary and tertiary structure predictions were made using four algorithms freely available online, CPHModels 3.2 (www.cbs.dtu.dk/services/CPHmodels, [20]), Fold and Function Assignment System (FFAS; ffas.ljcrf.edu, [21]), I-Tasser (zhang.bioinformatics.ku.edu/I-TASSER, [22]), and Phyre (www.sbg.bio.ic.ac.uk/~phyre, [23]). Each of the algorithms used are based on homology modeling rather than *ab initio* calculations and were selected because they all fared well in the past several years in the Critical Assessment of Techniques for Protein Structure Prediction (CASP), a world-wide competition to predict protein folding based on primary sequence information. The three-dimensional molecular viewer PyMOL (DeLano Scientific, LLC) was used to generate all crystal structure and homology model images shown. The program's "align" function was used to calculate alpha-carbon root-mean-square distances (RMSD) between crystal structures.

2.7 Western Blotting

SDS-PAGE analysis was performed using 4–15% precast linear gradient polyacrylamide gels (Bio-Rad, Hercules, CA). Proteins were either visualized by staining with Bio-Safe™ Coomassie G-250 Stain (Bio-Rad, Hercules, CA) or transferred to a Hybond™-P PVDF membrane (GE Healthcare-Biosciences, Piscataway, NJ) prior to analysis by Western blotting. Membranes were either incubated with a 1:5,000 dilution of polyclonal striped bass GST antisera [24, 25] or a 1:5,000 dilution of polyclonal channel catfish GST antisera [26] in 1X PBS-0.1% Tween containing 5% non-fat dried milk (Bio-Rad, Hercules, CA). Binding of the immobilized proteins was detected with 1:10,000 dilution of donkey anti-rabbit IgG antibody conjugated with horseradish peroxidase (Jackson ImmunoResearch, West Grove, PA) and enhanced chemiluminescence (GE Healthcare-Biosciences, Piscataway, NJ).

2.8 GST catalytic activity assays towards reference substrates and methyl parathion

Protein concentrations were measured by the Bradford method [27] using bovine serum albumin as the standard. The initial rate enzymatic activities of coho hepatic cytosolic GST toward the reference substrates CDNB, ECA, CuOOH, and DCNB were determined using a SpectraMax190 UV-vis 96-well microplate reader after determining pH optima for each substrate [9, 25]. All catalytic activity assays were performed at 30 °C and corrected for non-enzymatic activity. Analysis of GSH-dependent thiol oxidoreductase was determined spectrophotometrically using 2-HEDS after pH optimization of initial rate kinetics [28]. The rate of GST-mediated dealkylation of methyl parathion was measured by HPLC as previously described [9]. All samples were conducted in triplicate with mouse cytosol used as a positive control and denatured coho cytosol used to quantitate non-enzymatic activity. All catalytic activity assays followed initial rate kinetics.

2.9 LC/MS kinetic analysis of GST-catalyzed HNE conjugation

Kinetic parameters for HNE metabolism were determined as described previously [18]. Briefly, purified enzyme was incubated with 1 mM GSH and 10–150 μM HNE for 30 sec at

30 °C before quenching with 10 mM cysteine. Samples were analyzed using LC/MS and quantitated by comparing the peak area to purified GSHNE.

3. Results

3.1 Cloning and sequence analysis of olfactory GST isoforms

OlfGST omega, *pi*, and *rho* cDNAs were cloned from coho salmon olfactory total RNA by RACE-PCR. The *OlfGST omega* cDNA (accession number: JX416476) is 1297 nucleotides (nt) in length and contains a 720 nt open reading frame (ORF) encoding 239 amino acid (aa), and has 153 nt of 5' UTR and a 3' UTR of 424 nt including a tailing signal (AATAAA) and a poly (A) tail. The *OlfGST pi* cDNA (accession numbers: JX416477) is 858 nt in length and contains a 627 nt ORF encoding 208 aa, and has a 3' UTR of 231 nt including a tailing signal and a poly (A) tail. The *OlfGST rho* cDNA (accession numbers: JX416475) is 1016 nt in length and contains a 681 nt ORF encoding 226 aa, and has 45 nt of 5' UTR and a 3' UTR of 290 nt including a tailing signal and a poly (A) tail.

Amino acid sequence comparisons revealed high sequence identities when compared with other fish GST isoforms (Figure. 1). For example, GST omega, pi, and rho isoforms shared 98, 97, and 96 % identity with Atlantic salmon (*Salmo salar*) GSTs and 70, 71, and 63 % identity with zebrafish (*Danio rerio*) GSTs. Additionally, phylogenetic analysis of GSTs from fish and mammals revealed pi, omega, and rho GSTs assembling into distinct clusters with pi and rho GSTs aggregating to form a sub-cluster (Figure 2).

3.2 Structural characterization of coho OlfGSTs-SDS-PAGE analysis and immunoblotting

Whole protein mass spectrometry determined the molecular weights of the GST omega, pi and rho subunits to be 29,950, 23,354, and 26,655 Da, respectively, compared to the calculated molecular weights of 27,631, 23,408, and 26,087 Da, respectively. In the case of GST rho, which has a molecular mass 0.075% higher than the calculated value, the increase is attributed to the 3–4 thrombin residues left after cleavage. GST omega and pi, which could not be separated from the His moiety (6 histidine tags) via thrombin cleavage, have molecular masses 0.4% and 0.2 % above the calculated values. SDS-PAGE analysis of purified OlfGST rho and omega proteins revealed single bands with molecular masses similar to the calculated molecular weights (Figure 3A). However, Coomassie staining revealed a trace amount of additional polypeptide that co-purified with OlfGST pi (Figure 3A).

In order to establish the cross-reactivity and immunochemical identity of OlfGSTs, Western blotting was performed using polyclonal GST antisera from striped bass [24, 25] and channel catfish [26]. The striped bass GST antisera recognized OlfGST rho class proteins but not OlfGST pi or omega (Figure 3B), whereas the catfish GST antisera recognized OlfGST pi class proteins but not OlfGST rho and omega (Figure 3C). In general, cytosolic OlfGSTs cross-reacted extremely well with the bass GST antisera (Figure 3B, Lane 2). By contrast, cytosolic OlfGST cross-reactivity with the catfish GST antisera was significantly less notable (Figure 3C, Lane 2).

3.3 Homology analysis

Three of the four homology modeling algorithms – I-Tasser, CPHModels 3.2 and FFAS – used the Antarctic clam *Laternula elliptica* GST rho (LeGST rho) crystal structure (PDB ID: 3QAV), as the most similar model when predicting a structure for OlfGST rho. The fourth, Phyre, ranked 3QAV as the sixth best model but calculated its homology with OlfGST rho at 43% identical, the highest homology in the top 20 structure hits calculated by the algorithm. For that reason as well as the fact that other protein-structure prediction

algorithms chose to base their models on 3QAV, the Phyre homology model used was the one based on 3QAV (Figure 4A). The RMSD between 3QAV and each of the homology models ranged from 0.191 to 1.741 Å. For comparison, the RMSD between two LeGST rho crystal structures (PDB IDs: 3QAV and 3QAW) was 0.250 Å.

For the pi-class OlfGST, the Phyre and I-Tasser algorithms chose crystal structures of human and murine GST P1-1, respectively, as the top-ranked bases for the homology models. The Phyre model RMSD was 0.231 Å from huGST P1-1 (PDB ID: 2PGT), and the I-Tasser model RMSD was 0.505 Å from mGST P1-1 (PDB ID: 1GLQ) (Figure 4B). Similarly, homology models for the OlfGST omega enzyme aligned very well to the human counterpart, huGST O1-1. Both Phyre and I-Tasser selected a huGST O1-1 structure (PDB ID: 1EEM) as the top-ranked basis for generating the model, and the RMSD between 1EEM and the models were 0 and 0.52 Å, respectively, for Phyre and I-Tasser (Figure 4C).

3.4 Catalytic properties of olfactory GST isoforms

Initial rate GST activities toward the substrates CDNB, CuOOH, DCNB, ECA and 2-HEDS are shown in Table 2. As observed, the rho- and pi-class GSTs were particularly active towards the prototypical GST substrate CDNB. The omega- and rho-class GSTs exhibited thiol oxidoreductase activity with 2-HEDS. Furthermore, GST rho was the only OlfGST isoform that catalyzed the reduction of CuOOH and the desmethylation of methyl parathion, a reaction catalyzed by only a few human and rodent GST isoforms [29]. Previous LC/MS analysis provided kinetic parameters for human GST conjugation of HNE [30] (Table 3). OlfGST rho had a relatively low K_M of 22 μM and a k_{cat}/K_M of 14 $\text{sec}^{-1} \text{mM}^{-1}$. By comparison, OlfGST pi had a k_{cat}/K_M of 2.3 $\text{sec}^{-1} \text{mM}^{-1}$, whereas OlfGST omega did not metabolize HNE. In human GSTs, the alpha-class enzymes huGST A4-4 and, to a lesser extent, huGST A1-1, account for the majority of HNE clearance. HuGST A4-4 has a K_M of $7 \pm 6 \mu\text{M}$ and a k_{cat}/K_M of $5000 \pm 4500 \text{sec}^{-1} \text{mM}^{-1}$, while huGST A1-1 has a K_M of $43 \pm 25 \mu\text{M}$ and a k_{cat}/K_M of $270 \pm 170 \text{sec}^{-1} \text{mM}^{-1}$. HuGST P1-1, a pi-class enzyme, shows significantly lower catalytic efficiency with HNE ($k_{\text{cat}}/K_M = 43 \pm 7 \text{sec}^{-1} \text{mM}^{-1}$). While two human omega-class GSTs are known, their kinetics of HNE metabolism have not been characterized to our knowledge.

The HNE activity of rho-class GSTs from six aquatic species were determined previously, four of which exhibited high activity toward this endogenous substrate [10, 11, 31, 32]. An alignment of the corresponding primary sequences and OlfGST rho is shown in Figure 5A. In contrast to coho salmon (*Oncorhynchus kisutch*), largemouth bass (*Micropterus salmoides*) [10], plaice [11, 32] and European eel (*Anguilla anguilla*) [31], rho-class GSTs of red sea bream (*Pagrus major*) [12, 33] and the invertebrate amphioxus (*Branchiostoma belcheri*) [34] have no detectable HNE activity. The amino acids unique to the sea bream and amphioxus rho GSTs are highlighted in grey. Additionally, ten amino acids were found only in the red sea bream rho GST when compared with the salmon, eel, bass and plaice rho sequences that possess HNE activity (Figure 5A).

4. Discussion

The nasal cavity in mammals receives exposures to a variety of xenobiotics and natural compounds and, as such, these tissues express a variety of xenobiotic-metabolizing enzymes with broad substrate specificities for compounds ranging from drugs, carcinogens, and steroid hormones to dietary components and environmental pollutants [23]. In rodents, olfactory GSTs catalyze GSH conjugation of several odorants and xenobiotics, including unsaturated aldehydes and ketones, as well as DNA-damaging epoxides [23]. Given the functional significance of maintaining olfactory function, it is surprising that there are so few studies characterizing the ability of the peripheral olfactory system of fish to

biotransform waterborne chemicals or their metabolites. Even transient losses of olfactory function that occur in salmon during acute waterborne chemical exposures can impair key behaviors such as predator avoidance, detection of prey, courtship, and homing to natal streams [14–17]. The fact that two of the three major salmon olfactory GSTs in the present study were able to effectively conjugate HNE, a lipid-peroxidation product with neurodegenerative and cell-signaling properties [35, 36], suggests that a function of olfactory GSTs may be in neuroprotection of the olfactory system.

As discussed, the rho GSTs have been most widely described in fish and eels, although there is a recent report of a rho-class GST identified in the Antarctic clam (*Laternula elliptica*) [37]. The rho-class GSTs probably originated in aquatic organisms at least 500 million years ago [34]. It is interesting that although most rho GST isoforms isolated from aquatic organisms have HNE activity, rho GSTs from some species, including red sea bream (*Pagrus major*) [12, 33] and amphioxus (*Branchiostoma belcheri*) lack HNE activity [34]. These studies suggest that minor differences in protein structure can markedly affect HNE catalytic specificity. In the present study, salmon OlfGST rho had a relatively low K_M of 22 μM and a k_{cat}/K_M of 14 $\text{sec}^{-1} \text{mM}^{-1}$. By comparison, OlfGST pi had a k_{cat}/K_M of 2.3 $\text{sec}^{-1} \text{mM}^{-1}$, whereas OlfGST omega did not metabolize HNE. This clearly places coho salmon GST rho with other fish GSTs that conjugate HNE. The fact that exposure to trace metals, which are potent inhibitors of salmon olfactory function, can further increase cellular HNE levels suggests that GST proteins that conjugate HNE may be especially important in protecting against olfactory injury during environmental conditions that facilitate oxidative stress in fish.

Our hypothesis of a key role for GST rho in maintaining olfactory function in salmon is supported by the fact that among the three major salmon OlfGSTs, GST rho was the most active isoform in conjugating three structurally prototypical GST substrates – CDNB, 2-HEDS and CuOOH – and also in carrying out the GSH-mediated demethylation of the organophosphate pesticide methyl parathion. Organo(thio)phosphate (OP) esters such as methyl parathion are among the most widely used classes of insecticides and are particularly potent inhibitors of olfactory function in salmonids [38, 39]. In insects, GSTs play an important role in OP resistance [28, 40, 41]; likewise, GST-mediated demethylation has been shown to occur in humans as well, particularly via a theta-class GST [37]. Although GST induction has been reported in several fish species exposed to OP esters (including methyl parathion), there is little information regarding the ability of fish GSTs to catalyze OP detoxification, either via conjugation or demethylation. The fact that OlfGST rho was able to demethylate methyl parathion in the present study and that it is highly expressed in other coho tissues [8] suggest that this isoform is of importance in protecting against OP-mediated injury in salmon.

Until recently, no crystal structure of a rho-class GST was available. Since OlfGST rho catalyzes HNE conjugation with a catalytic efficiency on the same order of magnitude as the human alpha-class enzyme GST A1-1, a question is whether the active site of the fish rho enzyme is homologous. The alacrity with which human alpha-class GSTs catalyze HNE conjugation has been attributed in part to the alpha-class C-terminal helix, several residues of which provide critical interactions with HNE [42–44]. A crystal structure of the alpha-class huGST A4-4 bound with glutathionyl 1,4-dihydroxynonan-1-ol (GSDHN), an uncyclized form of GSHNE, is available [42]. While a crystal structure of huGST A1-1 with an HNE conjugate or analog is not available, the crystal structure of the highly homologous huGST A1-1 with *S*-hexylglutathione bound [45] is very similar to that of the GSDHN-bound huGST A4-4 with an RMSD of 0.829 Å. In both structures, the amino-acid side chains of the C terminus that are directed toward the observed or expected binding site of the alkyl chain of HNE are largely hydrophobic in nature, suggesting that hydrophobic interactions

between the substrate and the alpha-class C terminus help position HNE for conjugation, a phenomenon that has been observed with other alpha-class substrates [46–48].

A crystal structure released in February 2012 for the Antarctic clam *L. elliptica* GST rho (LeGST rho), by contrast, shows a substrate-binding site quite different from that of the human alpha-class enzymes. In the LeGST rho crystal structures (PDB IDs: 3QAW and 3QAV), the C-terminal region is not an ordered helix in either the apo-form or the GSH-bound form and is oriented such that the C-terminal region is greater than 9 Å from the GSH binding site (Figure 6). Since the two crystal structures published so far do not include a hydrophobic substrate or a product analog, little is known about the mode of HNE binding in a rho-class GST. However, based on the homology models we have constructed, hydrophobic substrate interactions with the active site of rho-GSTs are likely to be very different from the interactions in alpha-class GSTs.

Another difference between the alpha- and rho-class enzymes is the catalytic residue. In alpha-class GSTs, the catalytic residue is a highly conserved tyrosine around position 9, whereas in LeGST rho and in the homology models of OlfGST rho, the catalytic residue appears to be Ser15 (Ser13 using the OlfGST rho numbering scheme). In huGST P1-1, the catalytic residues are known to be Tyr7 (the hydroxyl oxygen is 5.6 Å from the glutathionyl sulfur in PDB 18GS) and Tyr108 (the hydroxyl oxygen is 4.73 Å from the glutathionyl sulfur) [49]. These distances do not differ much from the models for OlfGST pi, which clearly indicate Tyr8 (the hydroxyl oxygen is 5.6 Å from the glutathionyl sulfur in the Phyre model) and Tyr109 (the hydroxyl oxygen is 4.8 Å from the glutathionyl sulfur in the Phyre model) as the catalytic residues.

Historically, it has been assumed that GST pi was the predominant GST isoform in salmonids [7, 8, 50]. GST pi was previously shown to be a major olfactory isoform in sockeye salmon [51], where it has substantial expression along with GSH in the dendritic and perinuclear regions of olfactory receptor neurons [51–53]. From a catalytic perspective, the pi-class GSTs detoxify a range of compounds, including DNA and RNA hydroperoxides, environmental carcinogens and their metabolites, and several organophosphate pesticides [4]. Many of these compounds have relevance to salmonids, which experience environmental, waterborne chemical exposures during migration or staging activities [54–56]. In our study, GST pi had a k_{cat}/K_M of $2.3 \text{ sec}^{-1} \text{ mM}^{-1}$ toward HNE, suggesting that GST pi may also be involved in olfactory signaling and/or protection against HNE olfactory injury.

Although generally not well characterized in aquatic organisms, omega-class enzymes are unusual in that they form a disulfide bond between the cysteinyl sulfur in GSH and a cysteine in the N-terminal domain. It has been postulated that this disulfide bond, which diminishes the nucleophilicity of the GSH sulfur, accounts for the relatively low catalytic activity omega-class GSTs show with most typical GST substrates [57]. Instead, they show higher catalytic activity as thiol-transferases, as in the GSH-dependent reduction of dehydroascorbate [57]. With this in mind, it is not surprising that OlfGST omega showed negligible activity with HNE. The omega-class GSTs exhibit the canonical GST fold, but, unlike other GSTs, the omega-class GSTs have a cysteine residue in their active site. Genetic variation is common in the omega-class GST genes in humans, and individuals with variant alleles that result in deficiency of glutathione S-transferase omega 1-1 (GSTO1-1) have been widely characterized [58]. Genetic linkage studies have shown associations between GSTO genes and the susceptibility to several neurodegenerative diseases [59]. These studies, along with the fact that salmon recombinant GST omega was active in the conjugation of several products of oxidative stress and exhibited GSH-dependent thiol

oxidoreductase activity similar to thioredoxins, substantiate the importance of GST omega in maintaining salmon neurological function.

In conclusion, the present study describes the cloning, expression, and function of the major olfactory GSTs in coho salmon, one of seven Pacific salmon species whose populations have declined due to urbanization [60]. The fact that the majority of surface waters from urban streams in the Northwest contain multiple pesticides as well as neurotoxic trace metals that interfere with olfactory behaviors underscores the need to further our understanding of the ability of the salmon olfactory system to detoxify and modulate these chemicals [61]. The facts that OlfGST rho, in particular, 1) is a major olfactory GST isoform that rapidly conjugates CDNB, 2) has considerable antioxidant activity via HNE conjugation, reduction of CuOOH, and thioredoxin-like oxidoreductase activity, and 3) is the only major olfactory GST that detoxifies methyl parathion, collectively suggest a particularly important role for this isoform in protecting olfactory function. With regard to the structures of these proteins, it should be noted that when multiple protein-folding algorithms produce the same model, the accuracy of that model is likely to be high [62]. While we do not have crystal structures of OlfGST rho, pi or omega, for each of the three isoforms, four protein-structure-prediction algorithms generated essentially the same model, suggesting that the actual structures of OlfGST rho, pi and omega are likely to be similar to those postulated.

Acknowledgments

This work was supported in part by the University of Washington Superfund Research Program [NIEHS P42ES-04696], National Institutes of Health Grants [NIHGM 62284 (WMA) and T32GM 07752 (LMS)], and the University of Washington Sea Grant Program, pursuant to National Oceanic and Atmospheric Administration Award No. NA10OAR4170057, Project R/OCEH-5. The authors appreciate the assistance of Dr. Brian Beckman and Abby Tillotson at NOAA fisheries, Seattle, WA, who provided the juvenile coho salmon for these experiments. The views expressed herein are those of the author(s) and do not necessarily reflect the views of NOAA or any of its sub-agencies.

References

1. Allocati N, Federici L, Masulli M, Di Ilio C. Glutathione transferases in bacteria. *FEBS J.* 2009; 276:58–75. [PubMed: 19016852]
2. Buetler TM, Gallagher EP, Wang C, Stahl DL, Hayes JD, Eaton DL. Induction of phase I and phase II drug-metabolizing enzyme mRNA, protein, and activity by BHA, ethoxyquin, and oltipraz. *Toxicol Appl Pharmacol.* 1995; 135:45–57. [PubMed: 7482539]
3. Zimniak, P. Substrate and reaction mechanism of GSTs. In: Awasthi, YC., editor. *Toxicology of Glutathione Transferases*. Boca Raton, FL: Taylor & Francis CRC Press; 2006. p. 71-102.
4. Hayes JD, Pulford DJ. The glutathione *S*-transferase supergene family: regulation of GST and the contribution of the isoenzymes to cancer chemoprotection and drug resistance. *Crit Rev Biochem Mol Biol.* 1995; 30:445–600. [PubMed: 8770536]
5. Hayes JD, Flanagan JU, Jowsey IR. Glutathione transferases. *Annu Rev Pharmacol Toxicol.* 2005; 45:51–88. [PubMed: 15822171]
6. Eaton D, Bammler T. Concise review of the glutathione *S*-transferases and their significance to toxicology. *Review Toxicol Sci.* 1999; 49:156–64.
7. Schlenk, D.; Celander, M.; Gallagher, E.; George, S.; James, M.; Kullman, S., et al. Biotransformation in Fishes. In: Di Giulio, RT.; Hinton, DE., editors. *The Toxicology of Fishes*. New York: CRC press; 2008. p. 153-234.
8. Espinoza HM, Williams CR, Gallagher EP. Effect of cadmium on glutathione *S*-transferase and metallothionein gene expression in coho salmon liver, gill and olfactory tissues. *Aquat Toxicol.* 2012; 110–111:37–44.
9. Trute M, Gallis B, Doneanu C, Shaffer S, Goodlett D, Gallagher E. Characterization of hepatic glutathione *S*-transferases in coho salmon (*Oncorhynchus kisutch*). *Aquat Toxicol.* 2007; 81:126–36. [PubMed: 17184855]

10. Doi AM, Pham RT, Hughes EM, Barber DS, Gallagher EP. Molecular cloning and characterization of a glutathione S-transferase from largemouth bass (*Micropterus salmoides*) liver that is involved in the detoxification of 4-hydroxynonenal. *Biochem Pharmacol.* 2004; 67:2129–39. [PubMed: 15135309]
11. Leaver MJ, Scott K, George SG. Cloning and characterization of the major hepatic glutathione S-transferase from a marine teleost flatfish, the plaice (*Pleuronectes platessa*), with structural similarities to plant, insect and mammalian Theta class isoenzymes. *Biochem J.* 1993; 292 (Pt 1): 189–95. [PubMed: 8503846]
12. Konishi T, Kato K, Araki T, Shiraki K, Takagi M, Tamaru Y. A new class of glutathione S-transferase from the hepatopancreas of the red sea bream *Pagrus major*. *Biochem J.* 2005; 388:299–307. [PubMed: 15610066]
13. Pham RT, Barber DS, Gallagher EP. GSTA is a major glutathione S-transferase gene responsible for 4-hydroxynonenal conjugation in largemouth bass liver. *Mar Environ Res.* 2004; 58:485–8. [PubMed: 15178070]
14. Sandahl JF, Baldwin DH, Jenkins JJ, Scholz NL. A sensory system at the interface between urban stormwater runoff and salmon survival. *Environ Sci Technol.* 2007; 41:2998–3004. [PubMed: 17533870]
15. Tierney KB, Baldwin DH, Hara TJ, Ross PS, Scholz NL, Kennedy CJ. Olfactory toxicity in fishes. *Aquat Toxicol.* 2010; 96:2–26. [PubMed: 19931199]
16. Scott GR, Sloman KA. The effects of environmental pollutants on complex fish behaviour: integrating behavioural and physiological indicators of toxicity. *Aquat Toxicol.* 2004; 68:369–92. [PubMed: 15177953]
17. Sloman KA, Baker DW, Wood CM, McDonald G. Social interactions affect physiological consequences of sublethal copper exposure in rainbow trout, *Oncorhynchus mykiss*. *Environmental toxicology and chemistry/SETAC.* 2002; 21:1255–63. [PubMed: 12069311]
18. Shireman LM, Kripps KA, Balogh LM, Conner KP, Whittington D, Atkins WM. Glutathione transferase A4-4 resists adduction by 4-hydroxynonenal. *Arch Biochem Biophys.* 2010; 504:182–9. [PubMed: 20836986]
19. Tamura K, Peterson D, Peterson N, Stecher G, Nei M, Kumar S. MEGA5: molecular evolutionary genetics analysis using maximum likelihood, evolutionary distance, and maximum parsimony methods. *Mol Biol Evol.* 2011; 28:2731–9. [PubMed: 21546353]
20. Nielsen M, Lundegaard C, Lund O, Petersen TN. CPHmodels-3.0--remote homology modeling using structure-guided sequence profiles. *Nucleic Acids Res.* 2010; 38:W576–81. [PubMed: 20542909]
21. Jaroszewski L, Rychlewski L, Li Z, Li W, Godzik A. FFAS03: a server for profile--profile sequence alignments. *Nucleic Acids Res.* 2005; 33:W284–8. [PubMed: 15980471]
22. Roy A, Kucukural A, Zhang Y. I-TASSER: a unified platform for automated protein structure and function prediction. *Nat Protoc.* 2010; 5:725–38. [PubMed: 20360767]
23. Kelley LA, Sternberg MJ. Protein structure prediction on the Web: a case study using the Phyre server. *Nat Protoc.* 2009; 4:363–71. [PubMed: 19247286]
24. Gardner JL, Doi AM, Pham RT, Huisden CM, Gallagher EP. Ontogenic differences in human liver 4-hydroxynonenal detoxification are associated with in vitro injury to fetal hematopoietic stem cells. *Toxicol Appl Pharmacol.* 2003; 191:95–106. [PubMed: 12946646]
25. Gallagher EP, Sheehy KM, Lame MW, Segall HJ. *In vitro* kinetics of hepatic glutathione S-transferase conjugation in largemouth bass and brown bullheads. *Environ Toxicol and Chem.* 2000; 19:319–26.
26. Gadagbui BK, James MO. Activities of affinity-isolated glutathione S-transferase (GST) from channel catfish whole intestine. *Aquat Toxicol.* 2000; 49:27–37. [PubMed: 10814804]
27. Bradford MM. A rapid and sensitive method for the quantitation of microgram quantities of protein utilizing the principle of protein-dye binding. *Anal Biochem.* 1976; 72:248–54. [PubMed: 942051]
28. Holmgren A, Aslund F. Glutaredoxin. *Methods Enzymol.* 1995; 252:283–92. [PubMed: 7476363]
29. Abel EL, Bammler TK, Eaton DL. Biotransformation of methyl parathion by glutathione S-transferases. *Toxicol Sci.* 2004; 79:224–32. [PubMed: 15103050]

30. Balogh LM, Roberts AG, Shireman LM, Greene RJ, Atkins WM. The stereochemical course of 4-hydroxy-2-nonenal metabolism by glutathione S-transferases. *J Biol Chem.* 2008; 283:16702–10. [PubMed: 18424441]
31. Carletti E, Sulpizio M, Bucciarelli T, Del Boccio P, Federici L, Di Ilio C. Glutathione transferases from *Anguilla anguilla* liver: identification, cloning and functional characterization. *Aquat Toxicol.* 2008; 90:48–57. [PubMed: 18804293]
32. Martinez-Lara E, Leaver M, George S. Evidence from heterologous expression of glutathione S-transferases A and A1 of the plaice (*Pleuronectes platessa*) that their endogenous role is in detoxification of lipid peroxidation products. *Mar Environ Res.* 2002; 54:263–6. [PubMed: 12408573]
33. Konishi T, Kato K, Araki T, Shiraki K, Takagi M, Tamaru Y. Molecular cloning and characterization of alpha-class glutathione S-transferase genes from the hepatopancreas of red sea bream, *Pagrus major*. *Comp Biochem Physiol C Toxicol Pharmacol.* 2005; 140:309–20. [PubMed: 15946636]
34. Fan C, Zhang S, Liu Z, Li L, Luan J, Saren G. Identification and expression of a novel class of glutathione-S-transferase from amphioxus *Branchiostoma belcheri* with implications to the origin of vertebrate liver. *Int J Biochem Cell Biol.* 2007; 39:450–61. [PubMed: 17084657]
35. Akude E, Zhrebetskaya E, Roy Chowdhury SK, Girling K, Fernyhough P. 4-Hydroxy-2-nonenal induces mitochondrial dysfunction and aberrant axonal outgrowth in adult sensory neurons that mimics features of diabetic neuropathy. *Neurotox Res.* 17:28–38. [PubMed: 19557324]
36. Hayes MA, Pickering DB. Comparative cytopathology of primary rat hepatocyte cultures exposed to aflatoxin B1, acetaminophen, and other hepatotoxins. *Toxicol Appl Pharmacol.* 1985; 80:345–56. [PubMed: 3927521]
37. Park H, Ahn IY, Kim H, Lee J, Shin SC. Glutathione S-transferase as a biomarker in the Antarctic bivalve *Laternula elliptica* after exposure to the polychlorinated biphenyl mixture Aroclor 1254. *Comp Biochem Physiol C Toxicol Pharmacol.* 2009; 150:528–36. [PubMed: 19651242]
38. Syvanen M, Zhou Z, Wharton J, Goldsbury C, Clark A. Heterogeneity of the glutathione transferase genes encoding enzymes responsible for insecticide degradation in the housefly. *J Mol Evol.* 1996; 43:236–40. [PubMed: 8703089]
39. Wang JY, McCommas S, Syvanen M. Molecular cloning of a glutathione S-transferase overproduced in an insecticide-resistant strain of the housefly (*Musca domestica*). *Mol Gen Genet.* 1991; 227:260–6. [PubMed: 2062307]
40. Akude E, Zhrebetskaya E, Roy Chowdhury SK, Girling K, Fernyhough P. 4-Hydroxy-2-nonenal induces mitochondrial dysfunction and aberrant axonal outgrowth in adult sensory neurons that mimics features of diabetic neuropathy. *Neurotox Res.* 2010; 17:28–38. [PubMed: 19557324]
41. Green N, Weech M, Walters E. Localization and characterization of glutathione-s-transferase isozymes alpha, mu, and pi within the mouse vomeronasal organ. *Neurosci Lett.* 2005; 375:198–202. [PubMed: 15694260]
42. Balogh LM, Le Trong I, Kripps KA, Shireman LM, Stenkamp RE, Zhang W, et al. Substrate specificity combined with stereopromiscuity in glutathione transferase A4-4-dependent metabolism of 4-hydroxynonenal. *Biochemistry.* 2010; 49:1541–8. [PubMed: 20085333]
43. Balogh LM, Le Trong I, Kripps KA, Tars K, Stenkamp RE, Mannervik B, et al. Structural analysis of a glutathione transferase A1-1 mutant tailored for high catalytic efficiency with toxic alkenals. *Biochemistry.* 2009; 48:7698–704. [PubMed: 19618965]
44. Nilsson LO, Gustafsson A, Mannervik B. Redesign of substrate-selectivity determining modules of glutathione transferase A1-1 installs high catalytic efficiency with toxic alkenal products of lipid peroxidation. *Proc Natl Acad Sci USA.* 2000; 97:9408–12. [PubMed: 10900265]
45. Le Trong I, Stenkamp RE, Ibarra C, Atkins WM, Adman ET. 1.3-A resolution structure of human glutathione S-transferase with S-hexyl glutathione bound reveals possible extended ligandin binding site. *Proteins.* 2002; 48:618–27. [PubMed: 12211029]
46. Maeda DY, Mahajan SS, Atkins WM, Zebala JA. Bivalent inhibitors of glutathione S-transferase: the effect of spacer length on isozyme selectivity. *Bioorg Med Chem Lett.* 2006; 16:3780–3. [PubMed: 16675217]

47. Dirr HW, Little T, Kuhnert DC, Sayed Y. A conserved N-capping motif contributes significantly to the stabilization and dynamics of the C-terminal region of class Alpha glutathione S-transferases. *J Biol Chem.* 2005; 280:19480–7. [PubMed: 15757902]
48. Bruns CM, Hubatsch I, Ridderstrom M, Mannervik B, Tainer JA. Human glutathione transferase A4-4 crystal structures and mutagenesis reveal the basis of high catalytic efficiency with toxic lipid peroxidation products. *J Mol Biol.* 1999; 288:427–39. [PubMed: 10329152]
49. Oakley AJ, Lo Bello M, Battistoni A, Ricci G, Rossjohn J, Villar HO, et al. The structures of human glutathione transferase P1-1 in complex with glutathione and various inhibitors at high resolution. *J Mol Biol.* 1997; 274:84–100. [PubMed: 9398518]
50. Dominey RJ, Nimmo IA, Cronshaw AD, Hayes JD. The major glutathione S-transferase in salmonid fish livers is homologous to the mammalian pi-class GST. *Comp Biochem Physiol B.* 1991; 100:93–8. [PubMed: 1756623]
51. Kudo H, Ueda H, Mochida K, Adachi S, Hara A, Nagasawa H, et al. Salmonid olfactory system-specific protein (N24) exhibits glutathione S-transferase class pi-like structure. *J Neurochem.* 1999; 72:1344–52. [PubMed: 10098835]
52. Starcevic SL, Zielinski BS. Immunohistochemical localization of glutathione S-transferase pi in rainbow trout olfactory receptor neurons. *Neurosci Lett.* 1995; 183:175–8. [PubMed: 7739787]
53. Tsujita T, Li L, Nakajima H, Iwamoto N, Nakajima-Takagi Y, Ohashi K, et al. Nitro-fatty acids and cyclopentenone prostaglandins share strategies to activate the Keap1-Nrf2 system: a study using green fluorescent protein transgenic zebrafish. *Genes Cells.* 2011; 16:46–57. [PubMed: 21143560]
54. Wentz DA, Bonn BA, Carpenter KD, Hinkle SR, Janet ML, Rinella FA, et al. Water quality in the Willamette Basin, Oregon, 1991–95. *US Geol Surv Circ.* 1998; 1161
55. Dubrovsky NM, Kratzer CR, Brown LR, Gronberg JM, Burow KR. Water quality in the San Joaquin – Tulare basins, California, 1992–1995. *US Geol Surv Circ.* 1998; 1159
56. Survey USG. *US Geol Surv Fact Sheet 097–99.* 1999. Pesticides detected in urban streams during rainstorms and relations to retail sales of pesticides in King County, Washington.
57. Board PG, Coggan M, Chelvanayagam G, Easteal S, Jermiin LS, Schulte GK, et al. Identification, characterization, and crystal structure of the Omega class glutathione transferases. *J Biol Chem.* 2000; 275:24798–806. [PubMed: 10783391]
58. Zhou H, Brock J, Casarotto MG, Oakley AJ, Board PG. Novel folding and stability defects cause a deficiency of human glutathione transferase omega 1. *J Biol Chem.* 2011; 286:4271–9. [PubMed: 21106529]
59. Board PG. The omega-class glutathione transferases: structure, function, and genetics. *Drug Metab Rev.* 2011; 43:226–35. [PubMed: 21495794]
60. Quinn, TP. *The behavior and ecology of Pacific salmon and trout.* Seattle: University of Washington press; 2005.
61. Hoffman RS, Capel PD, Larson SJ. Comparison of pesticides in eight US urban streams. *Environmental Toxicology and Chemistry.* 2000; 19:2249–58.
62. McGuffin, LJ. Protein Fold Recognition and Threading. In: Schwede, T.; Peitsch, MC., editors. *Computational Structural Biology.* Hackensack, NJ: World Scientific Publishing Company; 2008. p. 37-60.

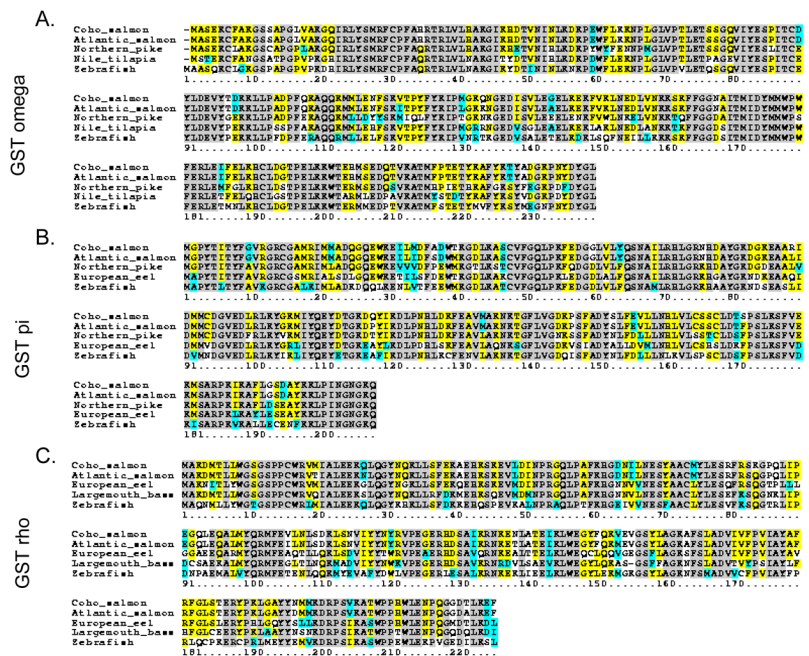


Figure 1. Amino acid sequence alignment of A) GST pi; B) GST omega; and C) GST rho
 Conserved residues shown in grey, identical residues in yellow, similar residues in cyan, and different residues in white.

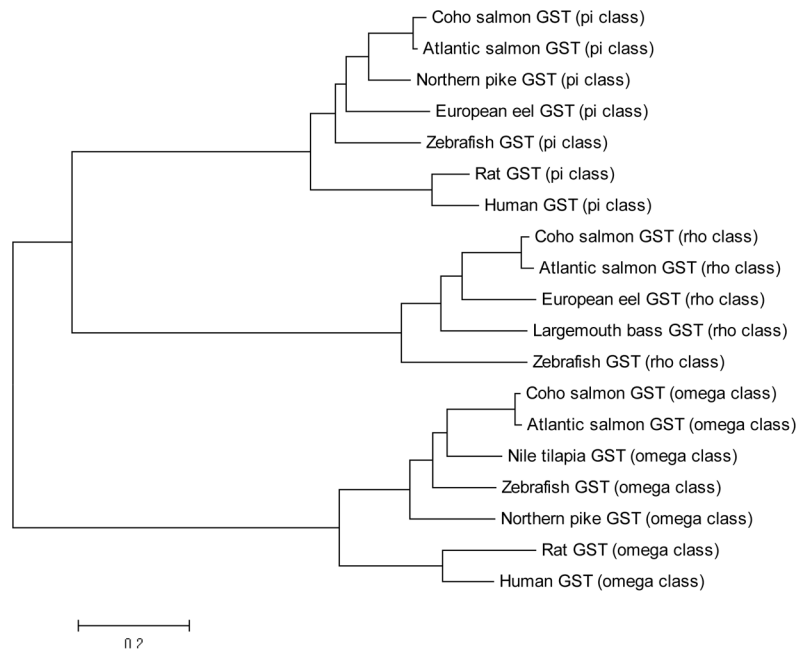


Figure 2. Phylogenetic analysis of reported GSTs from fish and mammalian species.

Tree was constructed by the NJ method using the MEGA 5.1 software. The amino acid sequences are coho salmon GST pi (*Oncorhynchus kisutch*, GenBank accession no. [JX416477](#)); 2: Atlantic salmon GST pi (*Salmo salar*, GenBank accession no. AC170112.1); 3: Northern pike GST pi (*Esox lucius*, GenBank accession no. ACO14315.1); 4: European eel GST pi (*Anguilla anguilla*, GenBank accession no. AAS01601.1); 5: zebrafish GST pi (*Danio rerio*, GenBank accession no. NP_571809.1); 6: Rat GST pi (*Rattus norvegicus*, GenBank accession no. NP_036709.1); 7: Human GST pi (*Homo sapiens*, GenBank accession no. AAC13869.1); 8: coho salmon GST rho (*Oncorhynchus kisutch*, GenBank accession no. [JX416475](#)); 9: Atlantic salmon GST rho (*Salmo salar*, GenBank accession no. ACM08643.1); 10: European eel GST rho, (*Anguilla anguilla*, GenBank accession no. ABY47336.1); 11: largemouth bass GST rho (*Micropterus salmoides*, GenBank accession no. AAQ91198.1); 12: zebrafish GST rho (*Danio rerio*, GenBank accession no. NP_001038525.1); 13: coho salmon GST omega (*Oncorhynchus kisutch*, GenBank accession no. [JX416476](#)); 14: Atlantic salmon GST omega (*Salmo salar*, GenBank accession no. NP_001134944.1); 15: Nile tilapia GST omega (*Oreochromis niloticus*, GenBank accession no. XP_003438319.1); 16: zebrafish GST omega (*Danio rerio*, GenBank accession no. NP_001002621.1); 17: Northern pike GST omega (*Esox lucius*, GenBank accession no. ACO13714.1); 18: Rat GST omega (*Rattus norvegicus*, GenBank accession no. NP_001007603.1); 19: Human GST omega (*Homo sapiens*, GenBank accession no. NP_004823.1).

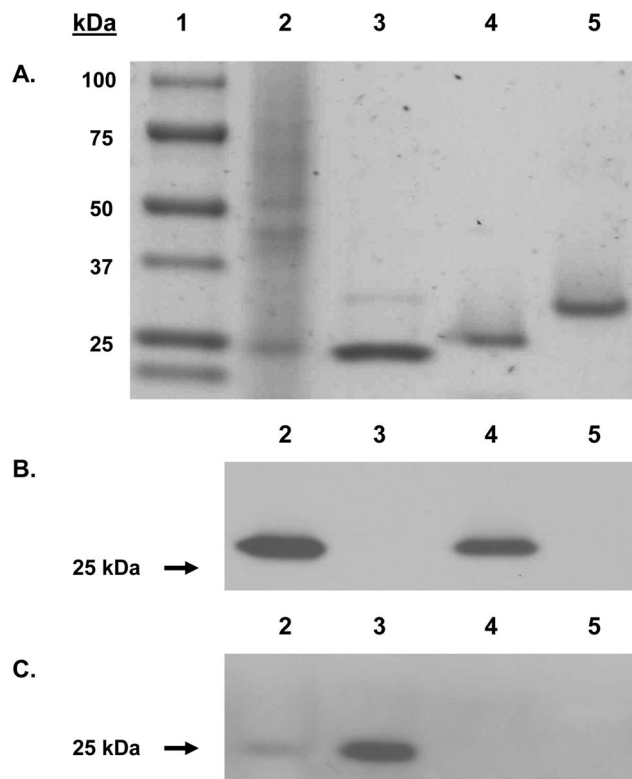


Figure 3. SDS PAGE and western blot analysis of coho salmon OlfGSTs
 (A). Samples were analyzed on a 4–15% gradient SDS-PAGE and proteins visualized by Coomassie Blue staining. Lane 1 contained the protein molecular weight standard; lane 2 contained coho salmon olfactory cytosol (10 µg); lanes 3–5 contained 2.5 µg of recombinant OlfGST pi, rho, and omega respectively. (B–C). Samples were blotted on PVDF membrane and probed with polyclonal GST antisera raised against striped bass GST that recognizes multiple GST forms, including rho of bass [24, 25] and also against a channel catfish GST pi antibody [26]. In both (B) and (C), lane 2 contained coho salmon olfactory cytosol (10 µg); and lanes 3–5 contained 2.5 µg of recombinant OlfGST pi, rho, and omega respectively.

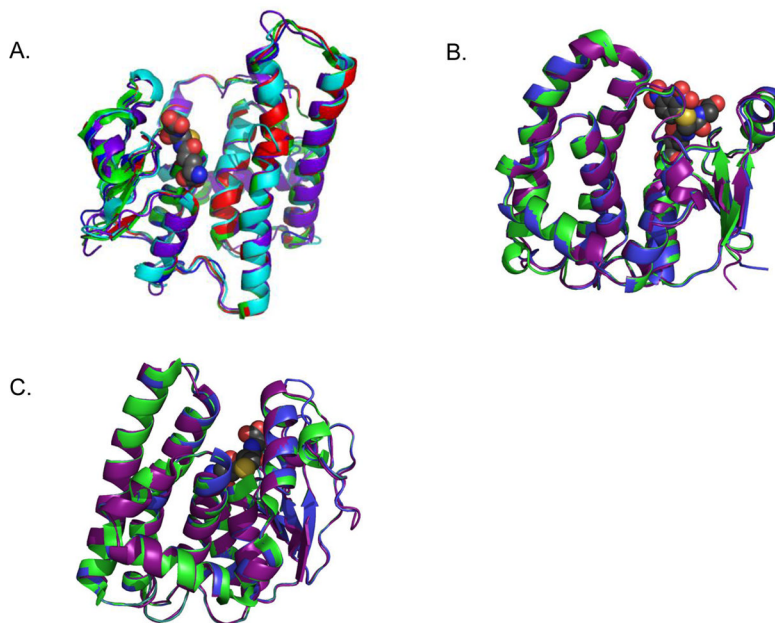


Figure 4. Homology analysis of coho OlfGSTs

(A). Alignment of LeGST rho (green, PDB 3QAW) and models for OlfGST rho from I-Tasser (purple), Phyre (blue), CPHModels 3.2 (cyan), and FFAS (red). Monomer shown for clarity. No model had a RMSD greater than 1.75 Å from the LeGST rho structure. Glutathione ligand from 3QAW shown as spheres, gray for carbon, yellow for sulfur, red for oxygen and blue for nitrogen (B). Alignment of huGST P1-1 (green, PDB 18GS) and models for OkGST pi from I-Tasser (purple) and Phyre (blue). Monomer is shown for clarity. Glutathionyl-dinitrobenzene ligand from 18GS shown as spheres, gray for carbon, yellow for sulfur, red for oxygen and blue for nitrogen. (C). Alignment of huGST O1-1 (green, PDB 1EEM) and models for OkGST omega from I-Tasser (purple) and Phyre (blue). Monomer shown for clarity. Glutathione ligand from 1EEM shown as spheres, gray for carbon, yellow for sulfur, red for oxygen and blue for nitrogen.

A.)

```

Salmon GST rho  MAKDMTLLWGSGPSPPCWRVMIALEEKQLQGYNQKLLSFEKAEHKSKEVLDINPRGQLPAF 60
Anguilla rho    MAKNITLWGSGPSPPCWRVMIALEEKQLQGYNGKLLSFEKQEHKSKEVMDINPRGQLPAF 60
Bass GST rho    MAKDMTLLWGSGPSPPCWRVQIALEEKSLQGYNQKLLRFDKMEHKSQEVMDMNPGRQLPAF 60
Seabream rho   MAKDMTLLWGSGPSPPCWRVMTLEEKNLQGYNQKLLSFEKMEHKSSEVVMKMNPRGQLPAF 60
Plaice rho     MAKDMTLLWGSGPSPPCWRVMTLEEKNLQAYNSKLLSFEKGEHKSAEVMSMNPGRQLPSF 60
Branchiost. rho MASDMTLWAGSGSPCWRAMICLEEKGLSDYNSKLLSFDNKEHKSDEVLKINPRGQMPTF 60

Salmon GST rho  KHGDNILNESYAACMYLESFRSRKGPQLIPEGQLEQALMYQRMFEVNLSDKLSN-VIYY 119
Anguilla rho    KHGNNVNESYAACLYLESQFRSQGTPLLLGGAEQARMYQRMFEAQTLLQKLSN-VIYY 119
Bass GST rho    KHGNNVNESYAACLYLESEFRSQGNKLI PDCSAEKALMYQRMFEGLTLAQKMD-VIYY 119
Seabream rho   KHGDKVNESYAACLYLENQFKSQGNKLI PDCPAELAMMYQRMFEGLSLAQKMD-VIYY 119
Plaice rho     KHGSKVNESYAACMYLESQFKSQGNKLI PDCPAEQAMMYQRMFEGLTLAQKMD-VIYY 119
Branchiost. rho KHGNÄIVNESFAICLYLENTFRGQAKLLPDDPVQALVLRQAVESQNIREKAAPGVLSY 120

Salmon GST rho  NYRVPEGERHDSAIKRKNENLATEIKLWEGYFQKVEVGSYLAKGAFSLADVIVFPVIAYA 179
Anguilla rho    TWRVPEAERHDSAVQRNKEALTTELKLWEGCLQVGEVGSFLAGKSFSLADVIVFPVIAYA 179
Bass GST rho    NWKVPEGERHDSAVKRNRDVLSAEVLWEGYLQKAS-GSFFAGKSFSLADVTVPYPSIAYL 178
Seabream rho   NWKVPEGERHDSAVKRNRSLTAEVLWEGYLQKTS-GGFLA-KTFSLADVQVYPSICYV 177
Plaice rho     SWKVPEAERHDSAVKRKNENLSTELKLWEEYLQKTS-GSFVAGKSFSLADVSVPFVAYL 178
Branchiost. rho FFRTKPEDRTEAMLEEKKKTCHHEELQIWEGYLÄRLGDGSYIAGKNFTLADACTFFFIATL 180

Salmon GST rho  FRFGLSTERYPKLGAYYNNMKDRPSVKATWPPHWLENPQGGDTLKEF 226
Anguilla rho    VRFGLSLERYPHLQYYSLKDRPSIKASWPPHWLENPQGMDTLKD 226
Bass GST rho    FHFGLCEERYPKLAAYNSLDRPSIKASWPPHWLENPQGGQDLKDI 225
Seabream rho   FRFGLCEERYPKLASYNSLDRPSIKASYPPHWLENPQGGQDLKDI 224
Plaice rho     FRFGLTEERYPQLTAYNSLKERPSIKASWPPHWLENPQGGQDLKDV 225
Branchiost. rho VRMGFNMSRYPHLAKYYDLVKDRPCVKASWPPHWKDTLN-KDVLKDI 226
    
```

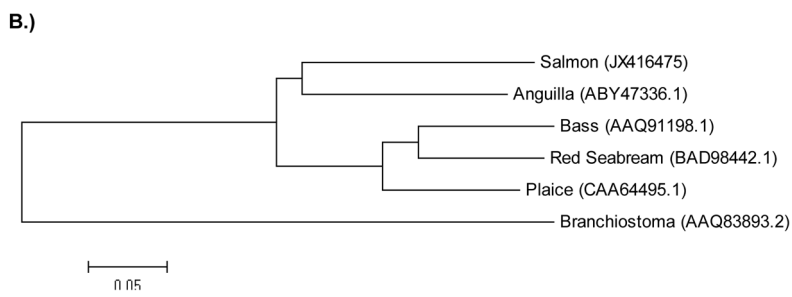


Figure 5. Sequence alignment and phylogenetic analyses of six rho class GSTs isolated from aquatic organisms
 (A). European eel, largemouth bass, plaice and coho rho GSTs possess HNE activity, whereas red sea bream and amphioxus (*Branchiostoma*) rho GSTs do not. Amino acids that distinguish the latter two rho GST sequences from the four HNE-conjugating forms are highlighted in grey. (B) Phylogenetic rooted-tree showing the relationship of coho GST rho with other aquatic rho-class GSTs. GenBank accession numbers are shown in parentheses. Tree was constructed by the Neighbor joining method (NJ) using MEGA 5.1 software.

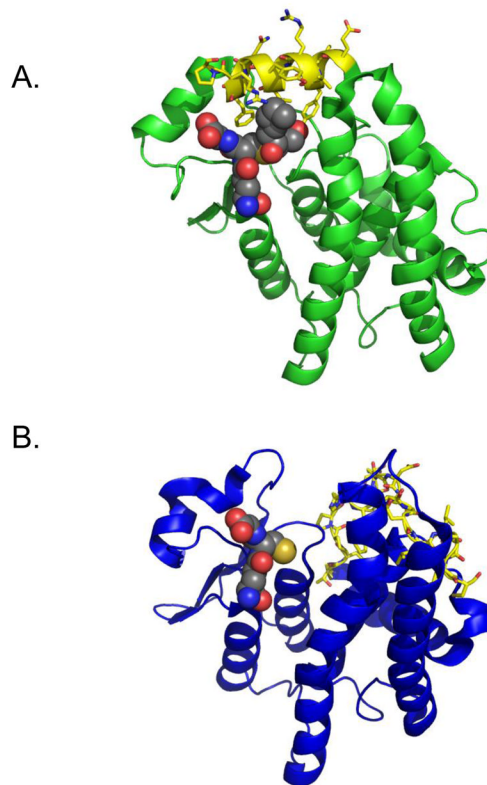


Figure 6. Crystal structures of (A) huGST A4-4 (PDB 3IK7) and (B) LeGST rho (PDB 3QAW) In both structures, C terminal residues are marked in yellow with sticks showing side chains. GSDHN (A44) or GSH (rho) are designated in spheres. The C terminus is far from binding site in rho (> 5 Å) but is critically involved in substrate binding in A4-4.

Table 1

Sequences of PCR primers used in this study.

Function	Primer (5' to 3')	Source Accession No.
<i>GST pi</i> 5' Race	Reverse: GGACGGGCTGACATCTTCTCGAC	BT059949.1
<i>GST pi</i> 3' Race	Forward: GTCAGCCCGTCCAAAATCAAGG	BT059949.1
<i>GST pi</i> full-length	Forward: CGGTAGCTAGCATGGGGCCATACACAATCACC	JX416477
	Reverse: GGCCCAAGCTTTCACGTGTTGCCATTGCC	
<i>GST rho</i> 5' Race	Reverse: TTCTGCGCCAGGTAAGAACCAC	BT073173.1 ; BT057296.1
<i>GST rho</i> 3' Race	Forward: GTGGGTCTTACCTGGCAGGAAA	BT073173.1 ; BT057296.1
<i>GST rho</i> full-length	Forward: CGGTAGCTAGCATGGCCAAGGACATGACACTTCTC	JX416475
	Reverse: GGCCCAAGCTTTCAGAACTCCTTGAGAGTGTC	
<i>GST omega</i> 5' Race	Reverse: TCCACTTCTCAGCTCAGGGGT	BT073404.1 ; BT049799.1
<i>GST omega</i> 3' Race	Forward: ACCCTGAGCTGAAGAAGTTGAC	BT073404.1 ; BT049799.1
<i>GST omega</i> full-length	Forward: CGGTAGCTAGCATGGCCTCTGAAAAATGTTTTCG	JX416476
	Reverse: GGCCCAAGCTTCTACAGGCCATAGTCATAATTGGG	

Table 2

Catalytic activities of the recombinant coho olfactory GST isoforms¹.

Isoform	CDNB	DCNB	ECA	CuOOH	2-HEDS	Methyl parathion*
GST rho	29,700	41	71	8	56	2.4
GST pi	1,236	6	124	BDL	BDL	<0.2 nmol/hr/mg
GST omega	71	1	12	BDL	61	<0.2 nmol/hr/mg

Key: 1-chloro-2,4-dinitrobenzene(CDNB), 1,2-dichloronitrobenzene (DCNB), ethacrynic acid (ECA), cumene hydroperoxide (CuOOH), and 2-diethylhexyl sulfide (2-HEDS). Units for GST enzymatic activities toward CDNB, DCNB, and ECA are nmol substrate conjugated/min/mg protein; GST-2-HEDS activity units are nmol 2-HEDS reduced/min/mg; GST-CuOOH units are nmol CuOOH reduced/min/mg; GST-methyl parathion units are nmol methyl parathion demethylated/hr/mg.

¹Data reported was obtained from three replicate analyses of enzymatic activities and displayed 10% variation.

Table 3

Catalytic properties of recombinant salmon olfactory GST isoforms toward 4-hydroxynonenal (HNE) (ND-not detected)

Isoform	K_m (mM)	V_{max} ($\mu\text{mol min}^{-1} \text{mg}^{-1}$)	k_{cat} (sec^{-1})	Catalytic Efficiency ($\text{sec}^{-1} \text{mM}^{-1}$)
OkGST omega	ND	ND	ND	0.34
OkGST pi	0.16 ± 0.06	0.5 ± 0.1	0.37 ± 0.09	2.3 ± 1.1
OkGST rho	0.028 ± 0.008	0.47 ± 0.05	0.41 ± 0.05	14 ± 4
huGST A1-1 WT	0.033 ± 0.008	2.0 ± 0.2	1.7 ± 0.2	52 ± 14
huGST A4-4 WT	0.034 ± 0.003	121.6 ± 4.7	100.1 ± 3.9	2953 ± 246